

RSC Advances



This is an *Accepted Manuscript*, which has been through the Royal Society of Chemistry peer review process and has been accepted for publication.

Accepted Manuscripts are published online shortly after acceptance, before technical editing, formatting and proof reading. Using this free service, authors can make their results available to the community, in citable form, before we publish the edited article. This *Accepted Manuscript* will be replaced by the edited, formatted and paginated article as soon as this is available.

You can find more information about *Accepted Manuscripts* in the [Information for Authors](#).

Please note that technical editing may introduce minor changes to the text and/or graphics, which may alter content. The journal's standard [Terms & Conditions](#) and the [Ethical guidelines](#) still apply. In no event shall the Royal Society of Chemistry be held responsible for any errors or omissions in this *Accepted Manuscript* or any consequences arising from the use of any information it contains.

Enhanced Light Sensing Performance of a Hybrid Device Developed Using As-grown Vertically Aligned Multiwalled Carbon Nanotubes on TCO Substrate

Mahananda Baro, Amreen A. Hussain, Arup R. Pal

Abstract

We report a suite of versatile plasma based methods for direct growth of vertically aligned multi-walled carbon nanotubes (MWCNTs) and MWCNT based hybrid composites on transparent conducting oxide (TCO) substrates. By using pulsed dc PECVD technique, short length vertically aligned MWCNTs are grown at 450 °C. The MWCNTs are uniformly distributed on TCO substrates with an average diameter and length of 49 ± 9 nm and 208 ± 26 nm, respectively. The area density of the vertically grown MWCNTs is as high as 7×10^9 cm⁻². The growth parameters are carefully refined to balance the tube dimension and density. Efforts have been made to synthesize MWCNTs based hybrid composites. The synthesized composites are discussed in terms of structural, morphological and optical properties. The as-fabricated MWCNT based hybrid composite is then utilized to show its applicability in self-powered hybrid photodetector. Interestingly, the photodetector shows an enhanced photoresponse at a very low incident power density of ~ 5.5 μWcm^{-2} . Utilization of a completely dry route for the synthesis and fabrication of MWCNT based hybrid composite emerge as a successful strategy suitable for hybrid nanocomposite material based advanced devices.

Introduction

Carbon based nanostructures have gained immense advances, in both experimental and theoretical fields.¹⁻³ Since the last two decades, different types of carbon nanostructures have been developed which includes carbon nanotube (CNT), carbon nanofiber (CNF), graphene, and fullerene.⁴⁻⁶ The properties of these nanostructured materials can be tuned depending upon their structures. The potentialities of CNT have given rise to an intense research activity to develop high quality materials based on CNT and their applicability in nano-device engineering. A remarkable progress has also been made in the development of innovative synthetic methodologies for growing superior quality CNTs. Apart from the best practices that are recognized worldwide for the synthesis of CNTs, there still remains a crucial challenge to actively control the alignment, area density, length and chirality of the CNTs. Different techniques have been opted for the synthesis of CNT structures which includes thermal chemical vapour deposition (T-CVD), catalytic chemical vapour deposition (CCVD), laser vaporization and arc discharges.⁷⁻¹⁰ Among these, plasma enhanced chemical vapour deposition (PECVD) provides an efficient alternative for low temperature production of CNTs.^{11, 12} It also gives the flexibility to grow vertically aligned CNT on various types of substrates.¹³

Generally, the synthesis of CNT is carried out on silicon substrates due to its high electrical and thermal stability but, in order to fit for various practical applications the controlled growth of CNT on suitable substrates is necessary such as transparent conducting oxide (TCO) substrates which are utilized in optoelectronic devices.^{14, 15} As for electrode configurations, CNT layers have been deposited on glass to replace TCO as the electrode material, yet it fails to attain a ratio between the sheet resistance and transparency which is the primary requirement of photo-sensing devices.¹⁶ Hybrid architectures with TCO and CNT are proved to be a promising strategy to improve the nano-structural and electrical properties of nano-devices.¹⁷ Literature reports on freestanding growth of CNT on TCO substrates often require high temperature growth (~ 600 °C), which represents a major obstacle to the conductivity and optical transmittance of the final electrode material.¹⁸ Therefore, exploration of alternative methods for direct growth of CNT on TCO substrates is necessary. Additionally, CNT based hybrid composites also provides a special class of nanostructured materials to be utilized for nano-device fabrication. Although transition metals and conducting polymers have been widely studied for different organic electronic applications, but only carbon based materials have displayed favourable flexibility and hence been promising in super-capacitors, electrochemical sensors and optoelectronic applications.¹⁹⁻²¹

In this work, we have explored the direct synthesis of vertically aligned multi-walled CNTs (MWCNTs) using pulsed dc PECVD on conducting Indium tin oxide (ITO) substrates. The method provides a feasible way towards direct growth of vertically aligned MWCNT on ITO substrates at 450 °C. Moreover, a hybrid composite material containing titanium dioxide (TiO_2) and plasma polymerized aniline (PPani) is prepared directly on the as-grown MWCNT/ITO substrates by plasma based routes. The MWCNT based hybrid composites are characterized and discussed in terms of structural, optical and morphological properties. Finally we have developed an UV-Visible photodetector based on the MWCNT based hybrid composite with enhanced photoresponse at a

low incident power density of $5.5 \mu\text{W}/\text{cm}^2$. The merits of utilizing a completely dry method for building such hybrid composites and photodetector provides a solvent-free and green technology towards the fabrication of large scale nano-devices without using any lithography based assembly.

Experimental details

Growth of vertically aligned MWCNT on TCO substrates

Vertically aligned MWCNT are produced by pulsed dc PECVD technique on ITO coated glass substrates. The detailed description of the plasma reactor is reported in a recent publication.²² Two protocols have been utilized for the synthesis of MWCNT.

The first protocol includes the preparation of catalyst. Initially, pulsed dc magnetron sputtering is used for the deposition of a thin Aluminium (Al) barrier layer of ~ 2 nm thickness on ITO substrate followed by post oxidation reaction process of Al layer to form alumina (Al_2O_3) by exposure of the substrates in ambient conditions for 24 hours. Further, the catalyst deposition is done by pulsed dc magnetron sputtering of Nickel (Ni) on top of alumina coated ITO substrates, thus maintaining a thickness of ~ 10 nm. Here, Ni acts as the CNT growth catalyst.

The second protocol involves the growth process of MWCNT using Ni/ Al_2O_3 /ITO geometry. First, the substrates with Ni/ Al_2O_3 /ITO configuration are treated with hydrogen (H_2) plasma accompanied by resistive heating at ~ 450 °C for 15 minutes. After 15 minutes of H_2 plasma treatment, Methane (CH_4) gas is slowly introduced in the plasma along with H_2 thus maintaining a gas ratio of 4:5 for H_2 : CH_4 , where CH_4 serves as a carbon precursor for CNT growth. The total process time for CNT growth is fixed at 45 minutes. The details of the experimental plasma conditions are summarized in table 1.

Device fabrication with MWCNT based hybrid composite

CNT based hybrid composites are prepared to show its applicability in hybrid photodetectors. The preparation of CNT based hybrid composite is systematically presented in the scheme shown in Fig. 1. The vertically aligned CNTs (C) are first grown by pulsed dc PECVD technique on ITO substrates. A 45 nm thick titanium dioxide (TiO_2) layer is then sputter deposited on top of the vertically aligned CNT (CT) followed by deposition of a 65 nm thick polymer layer by plasma polymerization of aniline monomer (PPani) to form CNT based hybrid composite. The final hybrid composite has the structure of CNT/ TiO_2 /PPani (CTP). The details of TiO_2 and PPani deposition by reactive magnetron sputtering and rf plasma polymerization are given in our recent publications as well as briefly summarized in table 1.²³⁻²⁵ For device fabrication, the CTP hybrid composite is deposited on ITO substrate by using proper masking arrangement, where ITO acts as the transparent conducting bottom electrode. After that, the CTP/ITO configuration is placed in a thermal evaporation chamber where high purity Al wire is evaporated on top of CTP/ITO

layout to form the top contact. The final device has the configuration of Al/PPani/TiO₂/CNT/ITO with an active surface area of 0.3 cm².

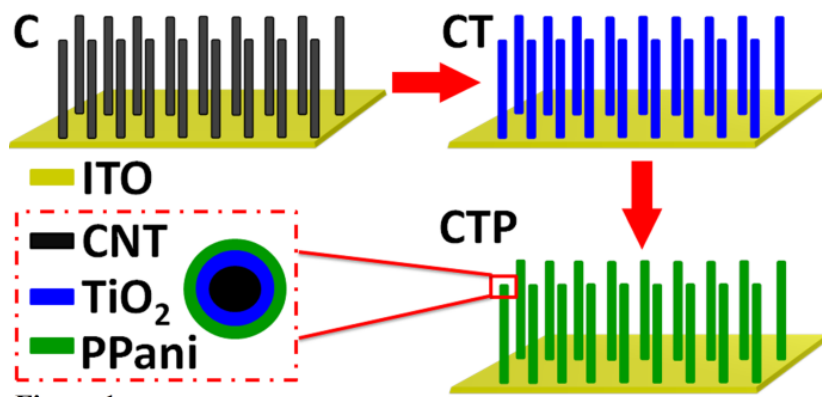


Figure 1

Figure 1: Schematic representation showing the preparation procedures for organizing CNT (C), CNT/TiO₂ (CT) and CNT/TiO₂/PPani (CTP) hybrid composites on Indium tin oxide (ITO) substrates using plasma based techniques.

Growth/ Synthesis parameters	CNT	TiO ₂	PPani
Growth/Deposition time (min)	30	40	0.5
Film thickness (nm)	-	45	65
Temperature (°C)	450	50	30
Working pressure (Torr)	3	0.008	0.1
Precursor gas	H ₂ , CH ₄	Ar, O ₂	Aniline
Power supply	Pulse DC	Pulse DC	RF
Discharge Power (W)	50	150	20
Duty cycle (%)	45	45	-
Frequency (Hz)	100 k	100 k	13.56 M
Negative self-bias (V)	-	-	23-34

Table 1: Discharge controlling parameters summarizing the synthesis of MWCNTs, deposition of TiO₂ thin films and deposition of plasma polyaniline thin films

In the device architecture, TiO₂ acts the n-type acceptor material while polyaniline acts as the p-type donor material forming the photoactive layer where charge carrier generation takes place. The photoactive layer is intentionally prepared on top of MWCNT arrays to increase the overall surface area of the device and enhancing the electrical conductivity of the hybrid composite.

Upon illumination (UV or Visible) with a photo-energy greater than the semiconductor band gap, excitons i.e. electron-hole pairs bound by Coulomb force are photo-generated at the bulk material. After that, charge separation occurs at the interface between the donor and acceptor material due to high electron affinity of the acceptor material (TiO_2). Subsequently, transport of charge through the bulk material takes place and finally collection of charges by the respective electrodes (ITO and Al) occurs, which results in the flow of current in the external load. Generally, in a hybrid system, TiO_2 nanoparticles are combined with PPani matrix to create a charge-transfer junction with a large interfacial area which will result in a greatly enhanced photoresponse of the device.

Sample characterizations

The morphology of the MWCNT grown on ITO substrates is first examined by field emission scanning electron microscopy (FESEM, SIGMA, Zeiss, Germany) imaging at high magnification with an extractor voltage of 5 kV, in which a uniform density of CNT is observed. The numbers of CNT are then roughly calculated based on high resolution top-view and cross-sectional FESEM images that can identify a single CNT clearly. In this work, the CNT numbers are calculated from a fixed area of $\sim 1 \mu\text{m}^2$ of the top-view FESEM image under high magnification. The average diameter and length of CNTs are analyzed by the software ImageJ (National Institute of Health, USA). Transmission electron microscopy (TEM, JEOL JEM 2100, Japan) operating at 200 kV is utilized to analyze CNT and CNT based hybrid composite nanostructures. The CNTs and CNT hybrid composites are collected from the substrates and dispersed onto Cu TEM grids for HRTEM analysis.

Chemical structure of the resulting CNTs and CNT based hybrid composite films on ITO substrates are determined by FTIR (Nicolet 6700 FT-IR) operated in transmission mode. Ultraviolet-visible (UV-Vis) absorbance is recorded for CNTs and CNT based hybrid composite films deposited on ITO substrates by UV-Vis Spectrophotometer (UV-1601, Shimadzu, Japan) to study the optical properties of the films. Individual film thicknesses are measured by X-Ray reflectivity (XRR) (D8 Advance, Bruker, Germany). The electrical measurements of the fabricated device using CNT based hybrid composite is carried out using a voltage source meter (KEITHLEY 6517B electrometer) and the photoresponse is characterized using a UV and Visible light illumination under ambient conditions. All the measurements are carried out after the exposure of the samples to atmosphere.

Results and Discussions

Surface morphology

The degree of substrate coverage by MWCNTs, their length, diameter and alignment is evaluated by FESEM analysis. Fig. 2(a) shows the cross-sectional view of randomly oriented MWCNTs which are directly grown on ITO substrate without using any barrier layer. In this case, the growth is not uniform over the substrate. The low density of MWCNT is due to high diffusion rate of catalyt on ITO substrate which ultimately resulted in slow nucleation rate for prominent CNT growth.²⁶ In order to further

improve the structure of CNTs, a barrier layer of Al_2O_3 is used which prevents the catalyst diffusion. Fig. 2(b) presents the FESEM micrograph of MWCNTs which are grown directly on ITO substrates using Al_2O_3 as the barrier layer. A uniform growth with reasonable area density of $7 \times 10^9 \text{ cm}^{-2}$ is observed. The inclusion of a very thin Al_2O_3 barrier layer of $\sim 2 \text{ nm}$ facilitates the aligned and uniform growth of CNTs. Moreover, the pulsed dc PECVD gave rise to direct growth of vertically aligned and dense MWCNTs on ITO substrates at $450 \text{ }^\circ\text{C}$. The diameter and length distribution of MWCNTs are shown in Fig. 2(c, d). The calculated average diameter and length of MWCNTs are $49 \pm 9 \text{ nm}$ and $208 \pm 26 \text{ nm}$, respectively where the diameter and length can be controlled to a large extent depending upon the catalyst film thickness and growth time.²²

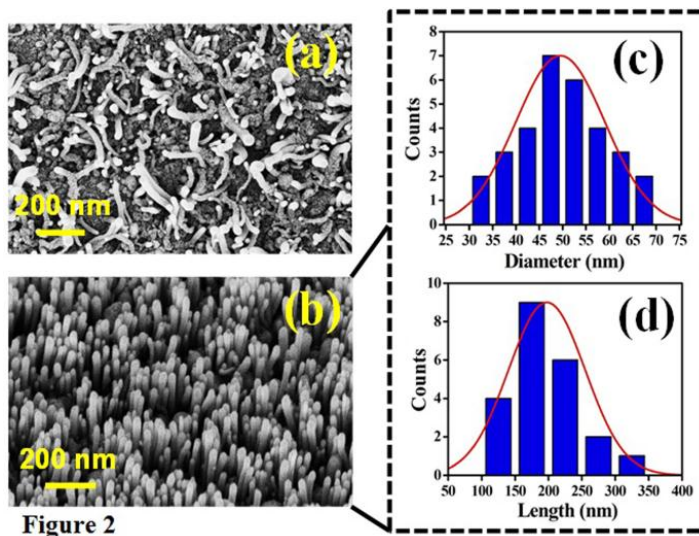


Figure 2

Figure 2: FESEM images of (a) randomly oriented CNTs on ITO substrate without using barrier layer (b) vertically aligned CNTs on ITO substrates with Al_2O_3 barrier layer (c) Diameter and (d) length distributions of vertically aligned CNTs

In case of MWCNTs, the graphene layers are parallel to the tube axis¹² which is further confirmed from the HRTEM analysis which provides more insight into the structural and morphological properties of MWCNTs. HRTEM images in Fig. 3(a) and 3(b) shows the morphology of a typical MWCNT and the corresponding graphitic walls. The MWCNT show some well-graphitized area with their basal planes oriented parallel to the tube axis with a central hollow region. The degree of crystallinity of MWCNT is low which evidenced the presence of defect states in CNT. The experimental lattice spacing of 0.34 nm is calculated, which is consistent with the d values of (002) plane for graphitic interlayer of MWCNT.²⁷

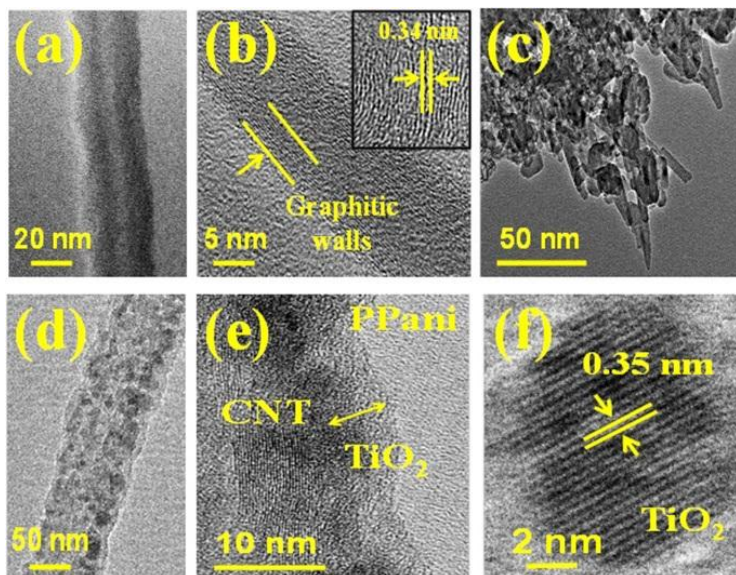


Figure 3

Figure 3: HRTEM images of (a) MWCNT (b) magnified image of MWCNT showing the graphitic walls. *In the inset*, the corresponding lattice fringes of CNT are shown (c) MWCNT based hybrid composite (d) MWCNT coated with TiO₂ (e) MWCNT coated TiO₂ and PPani (f) lattice fringes of TiO₂

Further, Fig. 3 also includes the HRTEM images of MWCNT based hybrid composite. A typical image containing CNT, TiO₂ and PPani is shown in the first image (Fig. 3(c)) which clearly distinguished the presence of MWCNTs coated with TiO₂ and PPani. In the second image a magnified view of MWCNT coated with TiO₂ is presented (Fig. 3(d)) where the TiO₂ nanoparticles are distributed on the walls of MWCNTs. Moreover, a magnified image of MWCNT/TiO₂/PPani hybrid composite is distinctly shown in Fig. 3(e) where the presence of TiO₂ is found outside the graphitic walls of MWCNT. In addition, PPani matrix is uniformly distributed in the background to form a thin film. The presence of TiO₂ in the hybrid composite material is inferred by direct visualization of lattice fringes in HRTEM micrographs. Fig. 3(f) clearly shows the lattice fringes of TiO₂ nanoparticle with 0.35 nm lattice spacing corresponding to the *d* values of (101) plane of anatase TiO₂ nanoparticle.²⁸

Structural and optical properties

FTIR transmittance spectra of MWCNTs and CTP hybrid composite are presented in Fig. 4(a). A weak band at 1584 cm⁻¹ is observed which is attributed to infra-red active graphite like E_{1u} mode, also known as G band which originates from the sp² hybridized carbon.²⁹ The bands at 1729 cm⁻¹ and 3000 cm⁻¹ are assigned to COOH and C-H_x groups.^{29, 30} The defect related peak of MWCNTs is obtained at 1234 cm⁻¹, which is attributed to the defect states on the walls of CNTs, consistent with the results obtained from HRTEM.³⁰ In addition, Raman analysis of MWCNTs is performed and is presented in figure S1 (ESI). By comparison, the FTIR spectrum of CTP presents several additional peaks thus supporting the presence of PPani and TiO₂ in the

hybrid composite. The band positions at 1602 cm^{-1} and 1498 cm^{-1} are assigned to C=C stretch of quinoid (Q) and benzenoid (B) units of the polymer which are able to sustain in the composite. The peak positions of the two main units of the polymer (benzenoid and quinoid) are shifted when compared with the reported results in plasma polyaniline which indicates the interaction of PPani and MWCNTs.²⁵ The appearance of the band at 1310 cm^{-1} assigned to C–N stretch suggests the aromatic linkages.^{23, 24} Moreover, the absorption band at 723 cm^{-1} is attributed to the anti-symmetric Ti–O–Ti stretch mode which evidences the incorporation of TiO_2 into the polymer matrix as well as to the MWCNT surface.²⁴ These results strongly support the formation of MWCNT based hybrid composite. Fig. 4(b) presents the UV-Vis spectra of MWCNTs and CTP hybrid composite. The MWCNTs show one sharp absorption band at 235 nm. A significant red-shift in the absorption is observed for the CTP hybrid composite as compared to MWCNTs. The amount of red-shift is quantified as $\Delta\lambda = +70\text{ nm}$. This noticeable red-shift may be ascribed to the bonding and interaction among CNTs and $\text{TiO}_2/\text{PPani}$ composite. The considerable amount of red-shift of this composite material implies that the material could be a potential candidate for ultraviolet as well as visible light sensing applications.

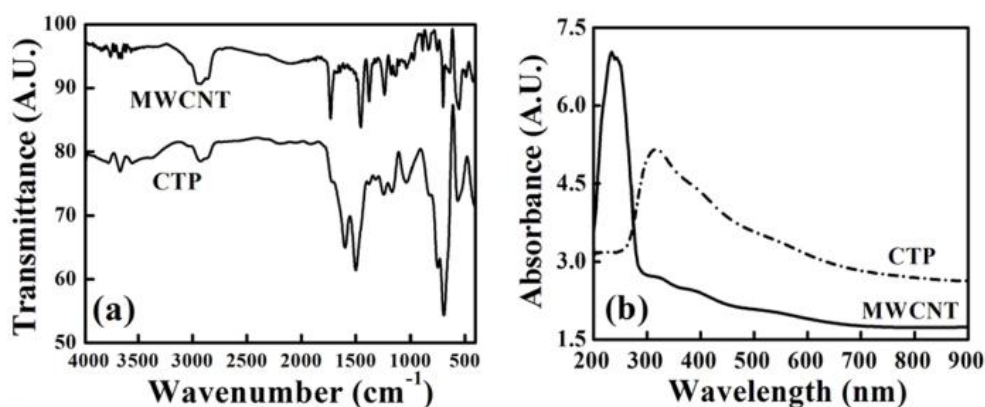


Figure 4

Figure 4: (a) FTIR transmittance spectra of MWCNT and MWCNT based hybrid composite with CNT/ TiO_2 /PPani (CTP) configuration (b) UV-Vis absorbance spectra of MWCNT and MWCNT based hybrid composite with CNT/ TiO_2 /PPani (CTP) configuration

Applicability of MWCNTs in hybrid photodetectors

The fabrication of nano-devices based on carbon nanostructures has attracted considerable attention owing to its large surface area and high mechanical strength. Fig. 5(a) represents the current density-voltage (J-V) characteristics of the MWCNT based hybrid photodetector under dark and 365 nm wavelength ultraviolet (UV) illumination at intensity of $16\ \mu\text{Wcm}^{-2}$. In the dark condition, the device shows a dark current of $0.07\ \mu\text{Acm}^{-2}$ at 1 V bias, while, upon UV-365 nm illumination the current increases, up to $4.5\ \mu\text{Acm}^{-2}$ at an applied bias voltage of 1 V. Similarly, Fig. 5(b) shows the J-V characteristics of the device, measured

under dark and white light illumination with wavelengths within the range of 400-600 nm at $16 \mu\text{Wcm}^{-2}$. At this condition, a maximum photocurrent of $0.64 \mu\text{A/cm}^2$ is recorded at a bias voltage of 1 V. To further demonstrate the photoresponse characteristics of the MWCNT based hybrid photodetector, we explored the photosensitivity measurements under UV and white light illuminations. The photosensitivity is calculated as I_p/I_d , where, $I_p = I_{\text{light}} - I_{\text{dark}}/I_{\text{dark}}$, which is measured for both UV and white light at $16 \mu\text{Wcm}^{-2}$. A maximum photosensitivity of 63.28 and 52.33 is calculated for UV and visible light intensities. The result suggests that the inclusion of MWCNT in the device geometry significantly contributes to the device performance at a very low incident power density of $16 \mu\text{Wcm}^{-2}$.

Interestingly, the J-V characteristics clearly show a photovoltaic effect in the presence of both UV and white light. The inset of Fig. 5(a) shows the logarithmic plot of the photocurrent versus applied voltage under UV-365 nm illumination. A small photovoltaic effect with an open circuit voltage ($V_{\text{OC}} = 26.4 \text{ mV}$) and short circuit current ($I_{\text{SC}} = 7.8 \text{ nAcm}^{-2}$) is recorded. For the case of white light illumination, a significant increase in $V_{\text{OC}} = 320 \text{ mV}$ and $I_{\text{SC}} = 56.8 \text{ nAcm}^{-2}$ is recorded whereas voltage generation is very insignificant for UV illumination. This result is well expected from the UV-Vis spectrum which shows a clear red-shift. The results point towards the feasibility of using MWCNT based hybrid composite under self powered mode. The open circuit voltage reported in this work is a factor of 3 higher than recently reported values for solution processed hybrid self powered UV/Visible photodetectors.³¹

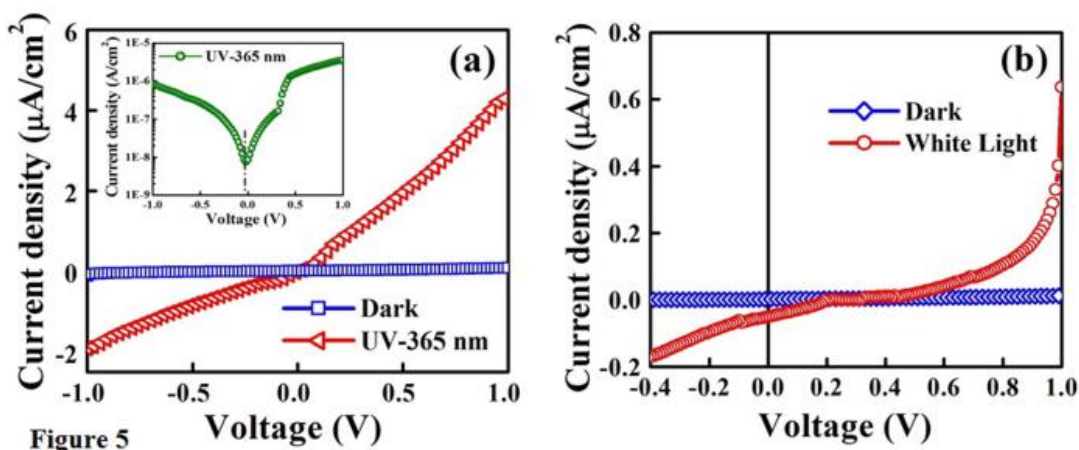


Figure 5: I-V characteristics of the hybrid photodetector at $16 \mu\text{Wcm}^{-2}$ under (a) UV-365 nm illumination (b) white light illumination

Since a significant photocurrent generation of the hybrid photodetector is recorded under UV illumination, therefore, a detailed response characteristic of the device is evaluated for UV illumination only. Fig. 6(a) shows the photocurrent plot at different incident light intensities under UV illumination. When intensity of the incident light is changed, the photocurrent of the hybrid device changed accordingly, which can be attributed to the change in the photon intensity, where light can be absorbed through

the whole thickness of the device so that both type of carriers can run within the device. Also, this result is consistent with the fact that charge carrier photogeneration efficiency is proportional to the absorbed photon flux. It should be noted that high photon flux can lead to saturation of the photocurrent versus excitation intensity.³² Therefore, this work presents the low light sensitivity down to $5.5 \mu\text{Wcm}^{-2}$ of the hybrid photodetector which is again one of the lowest excitation intensity utilized for self-powered hybrid photodetectors.^{31, 33, 34}

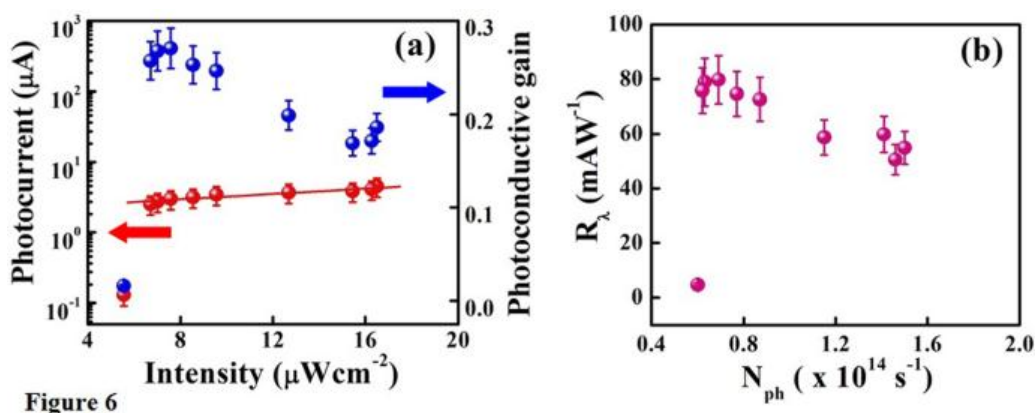


Figure 6: (a) Intensity dependent photocurrent and photoconductive gain (b) Responsivity as a function of absorbed photons of the hybrid photodetector under UV-365 nm illumination. The error bars represent the standard deviation of multiple measurements for different light intensities

On the basis of the dependence of photocurrent over UV light intensity and photon flux, a more quantitative analysis of the MWCNT based hybrid photodetector has been done, including photoconductive gain (G) and Responsivity (R_λ). These are the key parameters to evaluate the sensitivity of the hybrid photodetectors. The photoconductive gain (G) is defined as the increase in the number of collected carrier per absorbed photon with an energy $h\nu$ and can be expressed as:

$$G = (I_p / q) / (P / h\nu) \quad (1)$$

where I_p is the photocurrent, q is the elementary charge and P is the incident power on the active area of the device. The maximum photoconductive gain of $G = 0.27$ is achieved for the hybrid photodetector as shown in figure 6(a). Meanwhile, in order to examine the response of the photocurrent to incident optical power, the responsivity (R_λ) of the device is calculated following the expression:

$$R_\lambda = I_p / P \quad (2)$$

Additionally, the number of absorbed photons (N_{ph}) for a particular group of MWCNT is calculated which is given as:

$$N_{ph} = (P \times 2\pi \times r \times L \times n) / hv \quad (3)$$

where P is the incident power density in Wcm^{-2} , $r = 24.5$ nm and $L = 208$ nm are the radius and length of individual MWCNT between the electrodes and n is the number of MWCNT covering the active area of the hybrid device ($\sim 2 \times 10^9$). R_x as a function of N_{ph} is plotted in Fig. 6(b). The UV responsivity of 79.8 mAW^{-1} is achieved for the hybrid device which is at least a factor of 5-8 higher than the previous reports.^{31,33} High responsivity enables the use of hybrid device for sensing low light intensity.

Conclusion

We have successfully demonstrated the direct synthesis of vertically aligned MWCNTs on TCO substrates at 450°C . Optimal pulsed dc PECVD parameters are selected, making it possible to obtain short length and dense vertically aligned MWCNTs on TCO substrates. In addition, we have synthesized MWCNT based hybrid composites. The incorporation of TiO_2 , PPani and MWCNT is confirmed from FTIR and UV-Vis studies. A clear red-shift of the UV-Vis spectrum of the hybrid composite suggests its applicability for UV-Visible photo-sensing applications. Utilizing the hybrid composite, we have fabricated a self-powered hybrid UV-Visible photodetector. The as-fabricated device shows an enhanced photoresponse at a very low incident power density. Interestingly, the photo-sensing parameters are superior to the previous reports on self-powered hybrid UV-Visible photodetectors. It is concluded that the incorporation of MWCNTs in the device geometry improved the charge collection at the electrode thus, enhancing the photoresponse for self-powered operation.

Acknowledgement

Authors gratefully acknowledge the financial support from Council of Scientific and Industrial Research (CSIR), Government of India (Grant Number: 03(1198)/11/EMR-II). Authors are also thankful to SAIF-NEHU, Shillong for providing TEM characterization facility.

Notes

Physical Sciences Division, Institute of Advanced Study in Science and Technology, Paschim Boragaon, Garchuk, Guwahati-781035, Assam, India

*E-mail: arpal@iasst.gov.in, Phone: +91 361 2912073, Fax: +91 361 2273063

References

- 1 F. Léonard and A. A. Talin, *Nature Nanotech.*, 2011, **6**, 773
- 2 S. Iijima, *Nature*, 1991, **354**, 56
- 3 R. T. K. Baker, *Carbon*, 1989, **27**, 315
- 4 Y Lan, Y. Wang and Z. F. Ren, *Adv. Phys.*, 2011, **60**, 553
- 5 A. K. Geim and K. S. Novoselov, *Nat. Mater.*, 2007, **6**, 183
- 6 H. W. Kroto, J. R. Heath, S. C. O'Brien, R. F. Curl and R. E. Smalley, *Nature*, 1985, **318**, 162
- 7 C. E. Baddour, F. Fadlallah, D. Nasuhoglu, R. Mitra, L. Vandsburger and J. L. Meunier, *Carbon*, 2009, **47**, 313
- 8 J. Zhu, J. Jia, F-L. Kwong and D. H. L. Ng, *Carbon*, 2012, **50**, 2504
- 9 T. Guo, P. Nikolaev, A. Thess, D. Coldert and R. E. Smalley, *Chem Phys. Lett.*, 1995, **243**, 49
- 10 Y. Saito, *Carbon*, 1995, **33**, 979
- 11 H. Wang and Z. F. Ren, *Nanotechnology*, 2011, **22**, 405601
- 12 H. Wang and J. J. Moore, *Carbon*, 2012, **50**, 1235
- 13 S. Hofmann, C. Ducati, B. Kleinsorge and J. Robertson, *Appl. Phys. Lett.*, 2003, **83**, 4661
- 14 A. J. Miller, R. A. Hatton, G. Y. Chen and S. R. P. Silva, *Appl. Phys. Lett.*, 2007, **90**, 023105
- 15 Z. Li, H. R. Kandel, E. Dervishi, V. Saini, Y. Xu, A. R. Biris, D. Lupu, G. J. Salamo and A. S. Biris, *Langmuir*, 2008, **24**, 2655
- 16 A. D. Pasquier, H. E. Unalan, A. Kanwal, S. Miller and M. Chhowalla, *Appl. Phys. Lett.*, 2005, **87**, 203511
- 17 R. Ulbricht, S. B. Lee, X. Jiang, K. Inoue, M. Zhang, S. Fang, R. H. Baughman and A. A. Zakhidov, *Sol. Energ. Mat. Sol. Cells*, 2007, **91**, 416

- 18 H. T. Ng, B. Chen, J. E. Koehne, A. M. Cassell, J. Li, J. Han and M. Meyyappan, *J Phys. Chem. B*, 2003, **107**, 8484
- 19 M. T. Byrne and Y. K. Gun'ko, *Adv. Mater.*, 2010, **22**, 1672
- 20 X. Yan, Z. Tai, J. Chena and Q. Xuea, *Nanoscale*, 2011, **3**, 212
- 21 Z. Liu, J. Wang, D. Xie and G. Chen, *Small*, 2008, **4**, 462
- 22 M. Baro, D. Gogoi, A. R. Pal, N. C. Adhikary, H. Bailung and J. Chutia, *Chem. Vap. Deposition*, 2014, **20**, 1
- 23 B. K. Sarma, A. R. Pal, H. Bailung and J. Chutia, *J. Phys. D: Appl. Phys.*, 2012, **45**, 275401
- 24 A. A. Hussain, A. R. Pal, H. Bailung, J. Chutia and D. S. Patil, *J. Phys. D: Appl. Phys.*, 2013, **46**, 325301
- 25 A. A. Hussain, S. Sharma, A. R. Pal, H. Bailung, J. Chutia and D. S. Patil, *Plasma Chem. Plasma Process.*, 2012, **32**, 817
- 26 J. G. Céspedes, S. Thomasson, K. B. K. Teo, I. A. Kimloch, W. I. Milne, E. Pascual and E. Bertran, *Carbon*, 2009, **47**, 613
- 27 S. Halveg, C. L. Cartes, J. Sehested, P. L. Hansen, B. S. Clausen, J. R. R. Nielsen, F. A. Pedersen and J. K. Nørskov, *Nature*, 2004, **427**, 426
- 28 J. Gim, V. Mathew, J. Lim, J. Song, S. Baek, J. Kang, D. Ahn, S. J. Song, H. Yoon and J. Kim, *Scientific Reports*, 2012, **2**, 946
- 29 N. Kouklin, M. Tzolov, D. Straus, A. Yin and J. M. Xu, *Appl. Phys. Lett.*, 2004, **85**, 4463
- 30 Y. Qiao, C. M. Li, S. J. Bao and Q. L. Bao, *J. Power Sour.*, 2007, **170**, 79
- 31 O. Game, U. Singh, T. Kumari, A. Banpurhar and S. Ogale, *Nanoscale*, 2014, **6**, 503
- 32 X. Liu, L. Gu, Q. Zhang, J. Wu, Y. Long and Z. Fan, *Nat. Comm.*, 2014, **5**, 4007
- 33 S. M. Hatch, J. Briscoe and S. Dunn, *Adv. Mater.*, 2013, **25**, 867
- 34 P. N. Ni, C. X. Shan, S. P. Wang, X. Y. Liu and D. Z. Chen, *J. Mater. Chem. C*, 2013, **1**, 4445